Journal of Structural Biology 201 (2018) 221–236

Contents lists available at ScienceDirect

Journal of Structural Biology

journal homepage: www.elsevier.com/locate/yjsbi

Mapping of recent brachiopod microstructure: A tool for environmental studies

Facheng Ye[a,*], Gaia Crippa[a], Lucia Angiolini[a], Uwe Brand[b], GianCarlo Capitani[c], Maggie Cusack[d], Claudio Garbelli[e], Erika Griesshaber[f], Elizabeth Harper[g], Wolfgang Schmahl[f]

[a] Dipartimento di Scienze della Terra "A. Desio", Università degli Studi di Milano, Milan, Italy
[b] Department of Earth Sciences, Brock University, St. Catharines, Ontario L253AI, Canada
[c] Dipartimento di Scienze dell'Ambiente e di Scienze della Terra, Piazza della Scienza 4, 20126 Milano, Italy
[d] Division of Biological & Environmental Sciences, Faculty of Natural Sciences, University of Stirling, Stirling FK9 4LA, UK
[e] State Key Laboratory of Palaeobiology and Stratigraphy, Nanjing Institute of Geology and Palaeontology, Chinese Academy of Sciences, Nanjing, China
[f] Department fur Geo- und Umweltwissenschaften, Ludwig-Maximilians Universitat Munchen, Munich, Germany
[g] Department of Earth Sciences, University of Cambridge, Cambridge CB2 3EQ, UK

ARTICLE INFO

Keywords:
Biominerals
Micromorphometry
Ontogenetic variation
Geochemical and environmental proxies

ABSTRACT

Shells of brachiopods are excellent archives for environmental reconstructions in the recent and distant past as their microstructure and geochemistry respond to climate and environmental forcings. We studied the morphology and size of the basic structural unit, the secondary layer fibre, of the shells of several extant brachiopod taxa to derive a model correlating microstructural patterns to environmental conditions. Twenty-one adult specimens of six recent brachiopod species adapted to different environmental conditions, from Antarctica, to New Zealand, to the Mediterranean Sea, were chosen for microstructural analysis using SEM, TEM and EBSD. We conclude that: 1) there is no significant difference in the shape and size of the fibres between ventral and dorsal valves, 2) there is an ontogenetic trend in the shape and size of the fibres, as they become larger, wider, and flatter with increasing age. This indicates that the fibrous layer produced in the later stages of growth, which is recommended by the literature to be the best material for geochemical analyses, has a different morphostructure and probably a lower organic content than that produced earlier in life.

In two species of the same genus living in seawater with different temperature and carbonate saturation state, a relationship emerged between the microstructure and environmental conditions. Fibres of the polar *Liothyrella uva* tend to be smaller, rounder and less convex than those of the temperate *Liothyrella neozelanica*, suggesting a relationship between microstructural size, shell organic matter content, ambient seawater temperature and calcite saturation state.

1. Introduction

To understand climate change, it is important to estimate the long-term natural variability of environmental parameters such as seawater temperature, seasonality, pH and acidification in the recent and distant past. Biominerals, the hard parts produced by organisms for support and protection, are one of the best tools to use, as they are high-resolution archives of proxies reacting and recording environmental conditions prevailing during their growth.

Shells of marine invertebrates, such as brachiopods and bivalves, are considered excellent archives for reconstructing recent and past environmental conditions (e.g., Popp et al., 1986; Grossman et al., 1991; Parkinson et al., 2005; Angiolini et al., 2007, 2009; Brand et al., 2011; Schöne and Surge, 2012; Cusack and Huerta, 2012; Brocas et al., 2013; Crippa et al., 2016a; Garbelli et al., 2017). Brachiopod shells in particular are high resolution biomineral archives used to reconstruct global marine environments in the recent and deep past, because: 1) they record the physical and chemical composition of the seawater in which they live with no or limited vital effects (e.g., Parkinson et al., 2005; Brand et al., 2013, 2015); 2) they precipitate a low-Mg calcite shell, which is generally resistant to diagenetic alteration (Lowenstam, 1961; Brand and Veizer, 1980; Popp et al., 1986; Brand et al., 2011); 3) they are common in the Phanerozoic, especially during the Palaeozoic when they dominated benthic communities (Curry and Brunton, 2007); and, 4) they are low metabolic and physiologically unbuffered organisms sensitive to change in the physicochemical composition of the

* Corresponding author.
E-mail address: facheng.ye@unimi.it (F. Ye).

https://doi.org/10.1016/j.jsb.2017.11.011
Received 5 June 2017; Received in revised form 21 November 2017; Accepted 22 November 2017
Available online 23 November 2017

Table 1
Brachiopods for shell microstructural analyses. Name of the species, locality and depth, corresponding geographic coordinates, water temperature and salinity, as well as the shell succession of each specimen with corresponding ID number, type of valve and the number of SEM micrographs. D: Depth, T: temperature, S: salinity.

	Species	Locality and depth	Geographic coordinate	Temperature and salinity	Shell sequence	ID number	Valve	SEM micrographs number
Terebratulida	*Liothyrella uva*	TI: Trolval Island, Ryder Bay SI: Signy Island (D: 10m), Antarctica	67° 35.44' S, 68° 12.44' W (TI) 60° 43' S, 45° 36' W (SI)	T: -2/+2 °C, S: 34 PSU (TI & SI)	I, II layers	LUH1	ventral	40
						LUH2	ventral	28
						LUH3	ventral and dorsal	98
						LU	ventral	36
						LUV/LUD	ventral and dorsal	135
	Gryphus vitreus	Tuscan Archipelago (D: 140–160m between the Island of Pianosa and Montecristo), Tyrrhenian Sea, Italy	42° 26' N, 10° 04' E	T: 13–15 °C, S: 39 PSU	I, II, III layers	1D	ventral and dorsal	111
						GV	ventral and dorsal	81
						GV3	ventral and dorsal	68
						GV4	ventral and dorsal	132
						GV5	dorsal	14
	Liothyrella neozelanica	Doubtful Sound (D: 18m), New Zealand	45° 18' 00" S, 166° 58' 45" E	T: 11–17 °C, S: 34.8 PSU	I, II, III layers	1C	ventral and dorsal	144
						LZ	ventral and dorsal	288
						LN	ventral and dorsal	176
	Calloria inconspicua	Doubtful Sound (D: 18m), New Zealand	45° 18' 00" S, 166° 58' 45" E	T: 11–17 °C, S: 34.8 PSU	I, II layers	1CC	ventral and dorsal	27
						CI	ventral and dorsal	43
	Magasella sanguinea	Doubtful Sound (D: 18m), New Zealand	45° 18' 00" S, 166° 58' 45" E	T: 11–17 °C, S: 34.8 PSU	I, II layers	TS1	ventral and dorsal	157
Rhynchonellida	*Notosaria nigricans*	DS: Doubtful Sound (D: 18m) KP: Kaka Point (D: 2–15m), New Zealand	45° 18' 00" S, 166° 58' 45" E (DS) 46° 38' 66" S, 169° 78' 23" E (KP)	T: 11–17 °C, S: 34.8 PSU (DS) T: 14 °C, S: 34–35 PSU (KP)	I, II layers	1DC	ventral	41
						NN	ventral and dorsal	59
						NN1	ventral and dorsal	34
						NN2	ventral and dorsal	135
						NN3	ventral and dorsal	47

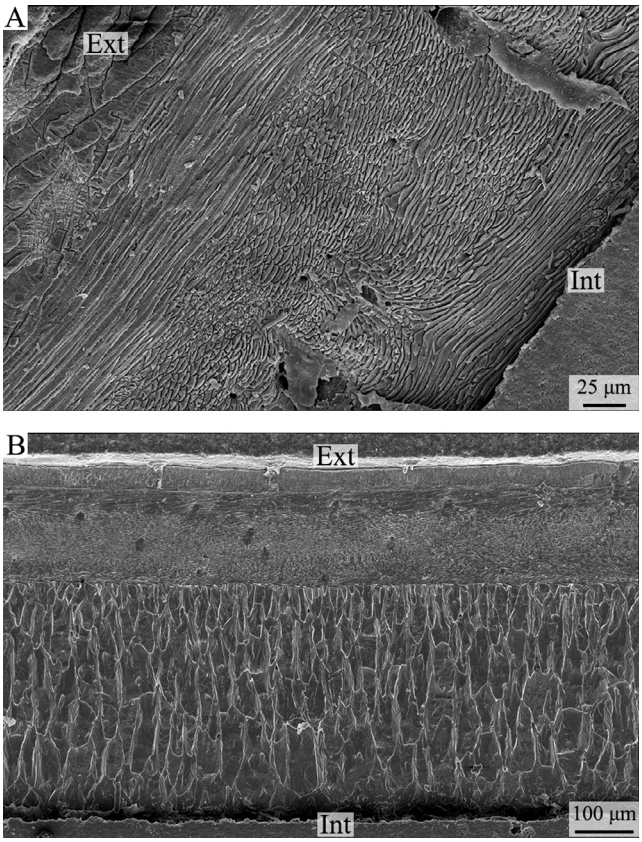

Fig. 1. A, shell structure of *L. uva*, made of primary microgranular and secondary fibrous layers; B, shell succession of *L. neozelanica* with primary microgranular layer, and secondary fibrous and tertiary columnar layers. Ext: external, Int: internal.

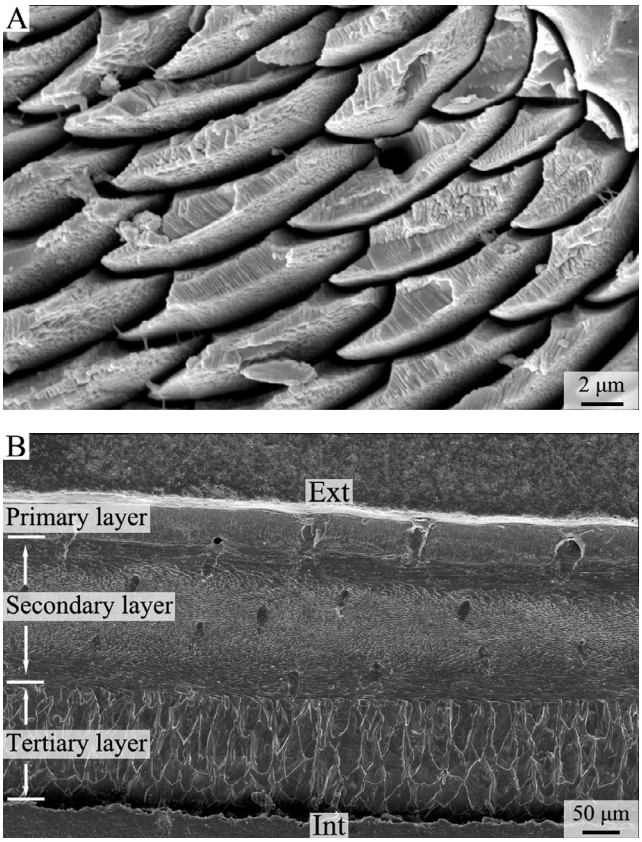

Fig. 2. *L. neozelanica*. A, enlarged photos showing fibres in transverse section (dorsal valve); B, complete shell succession showing change in the orientation of fibres from oblique to transverse from the exterior to the interior of the secondary layer (central part, ventral valve, longitudinal section). Ext: external, Int: internal.

ambient seawater (Peck et al., 1997; Peck, 2007).

Fossil biominerals have considerable potential for extending climate and environmental records on a broad geographical scale and over long periods of time (Garbelli et al., 2017). Recent brachiopods are unparalleled archives on how microstructure and geochemistry may respond or adapt to general or specific environmental conditions (Watson et al., 2012; Cross et al., 2016). Also, they allow for the study of complex relationships between different shell microstructures and the oceanographic geochemical record (e.g., Immenhauser et al., 2016).

Brachiopods possess complex microstructures (e.g., Schmahl et al., 2004; Griesshaber et al., 2007; Pérez-Huerta et al., 2009; Goetz et al., 2011; Gaspard and Nouet, 2016; Garbelli, 2017), but we focus on the fibres of the secondary layer of rhynchonelliformean brachiopods. Previous studies examined the nanostructure, hardness and orientation of the fibres within the secondary layer of extant brachiopods (e.g., Griesshaber et al., 2006; Pérez-Huerta et al., 2007; Goetz et al., 2009; Schmahl et al., 2012), but not the shape and size of individual fibres in different parts of the same shell and in different taxa. Here, we analyse the microstructure of six extant rhynchonelliformean brachiopods adapted to different environmental conditions, from Signy and Trolval Islands, Antarctica, to Doubtful Sound, New Zealand to the Tuscan Archipelago, Mediterranean Sea. We relate the observed patterns to 1) ontogenetic variation, and 2) environmental variables.

2. Materials

Six brachiopod species were chosen for shell microstructural analysis. A total of 21 adult specimens, of similar size, were investigated, all having a secondary shell layer. Sixty samples were cut along different longitudinal and perpendicular sections to investigate the size and shape of the fibres, the structural units of the secondary layer.

The analysed specimens belong to the terebratulid species *Liothyrella neozelanica* (Thomson, 1918), *Calloria inconspicua* (Sowerby, 1846), and *Magasella sanguinea* (Leach, 1814) from Doubtful Sound, New Zealand, *Liothyrella uva* (Broderip, 1833) from Trolval Island, Ryder Bay and Signy Island, Antarctica, and *Gryphus vitreus* (Born, 1778) from the Tuscan archipelago, Italy (Table 1). The rhynchonellid species *Notosaria nigricans* (Sowerby, 1846) comes from Doubtful Sound and Kaka Point, New Zealand (Table 1). Of these, *L. uva*, *C. inconspicua*, *N. nigricans* and *M. sanguinea* possess a shell consisting of primary microgranular and secondary fibrous calcite layer, whereas *L. neozelanica* and *G. vitreus* also have an additional tertiary columnar calcite layer (Figs. 1–3).

We used an array of methods to describe the microstructure of the fibres of the secondary layer. Fibre morphology was measured in sections cut perpendicular to the fibre axis at different positions of the same shell, while considering that brachiopod shells grow from the umbo (posterior) to the anterior margin and from the exterior to the interior (Fig. 4). We also considered that the secondary layer is constructed in sublayers characterized by different orientations of the morphological axis of the fibres (cf. Schmahl et al., 2004, 2008; Griesshaber et al., 2007, 2008, 2010; Goetz et al., 2011). Orientation of the fibres is complex in the posterior part of the shell, ranging from parallel to oblique and perpendicular to the growth vector, producing many sublayers (Plates 3–5 in Ye et al., 2017), but with fewer sublayers in their central and anterior regions. Specifically, *L. neozelanica* and *G. vitreus* have thin secondary and thick tertiary columnar layers, and the fibre axis in the most external and most internal sublayers is oriented obliquely to parallel to the growth vector (Griesshaber et al., 2008, 2010).

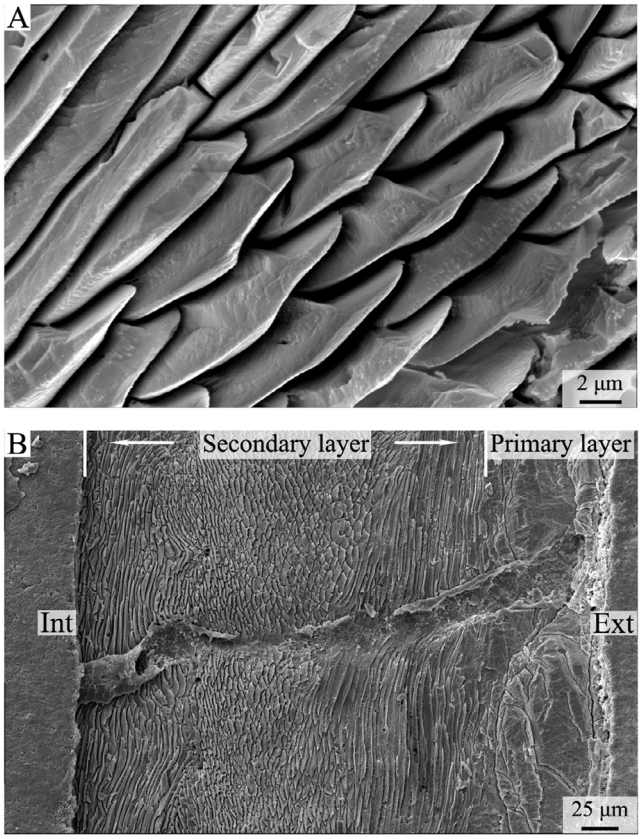

Fig. 3. A, *G. vitreus*. enlarged photo showing fibres in transverse section (ventral valve); B, *L. uva*. shell succession showing the change in the orientation of fibres from oblique to transverse to oblique from the exterior to the interior of the secondary layer (central part, ventral valve, longitudinal section). Ext: external, Int: internal.

3. Methods

We used Scanning electron microscope (SEM), Electron backscatter diffraction (EBSD), and Transmission electron microscope (TEM) to measure and evaluate size and shape of the structural units (fibres) within brachiopod shells, conducted data reliability analysis, and constructed a database for statistical analyses.

3.1. Sample preparation

We followed the preparation method suggested by Crippa et al. (2016b) for SEM analysis of specimens. Summarized here briefly, the specimens were embedded in epoxy resin, cut along the longitudinal axis, and immersed in 36 vol hydrogen peroxide (H_2O_2) for 24 h to remove organic matter. Sectioned surfaces were smoothed with silicon carbide powder (SiC), etched with 5% hydrochloric acid (HCl) for 3 s, and then rinsed in deionised water and dried. Then, they were gold-coated and observed by a Cambridge S-360 scanning electron microscope with a lanthanum hexaboride (LaB_6) source and operating at an acceleration voltage of 20 kV (Dipartimento di Scienze della Terra "A. Desio", University of Milan).

Electron Backscatter Diffraction (EBSD) measurements were performed on shells embedded in epoxy resin. The surface of the embedded specimen was subjected to several sequential mechanical grinding and polishing steps down to a grain size of 1 µm. The final step consisted of etch-polishing with colloidal alumina (particle size ~0.06 µm) in a vibratory polisher. For measurements, the samples were coated with 4–6 nm of carbon. EBSD measurements were carried out on a Hitachi SU5000 field emission SEM, equipped with a Nordlys II EBSD detector and AZTec acquisition software. The EBSD SEM was operated at 15 and 20 kV and measurements were indexed with the CHANNEL 5 HKL software (Schmidt and Olesen, 1989; Randle and Engler, 2000).

Information obtained from EBSD measurements is presented as band contrast images, and the grey scale gives the signal strength of the EBSD-Kikuchi diffraction pattern. The strength of the EBSD signal is high when a mineral is detected (bright), whereas it is weak or absent when the polymer is scanned (dark/black).

TEM mounts were prepared from epoxy embedded samples. In the first step, doubly polished petrographic thin sections (30 µm thick) were obtained by mechanical thinning. Electron transparency was then achieved by ion milling 3 mm wide discs cut out from the petrographic thin sections using a Gatan Precision Ion Polyshing System (PIPS) (Dipartimento di Scienze della Terra "A. Desio" of Milan). TEM mounts were finally carbon coated to avoid electrostatic charging. TEM observations were performed with a Jeol JEM 2010 operating at 200 kV and equipped with an Oxford Link energy dispersive spectrometer (EDS) and with an Olympus Tengra 2.3 k × 2.3 k × 14 bit slow-scan CCD camera (Dipartimento di Scienze Fisiche, della Terra e dell'Ambiente of the University of Siena).

3.2. Morphometric analysis

Based on SEM micrographs of the secondary layer, fibres with regular and symmetrical cross sectional outlines were chosen for morphometric measurement. It was assumed that fibres with a symmetric outline were cut perpendicular to the plane of symmetry of the fibres (Fig. 5A). For a single fibre, symmetric profiles (section perpendicular to the fibre axis) lead to smaller/narrower values (e.g., of area, perimeter, width) than asymmetric ones (Fig. 5C and D). However, even if cut perpendicular to the morphological axis of the fibres, small tilting of the section would result in a slightly larger area or perimeter (Fig. 5B), so that the most reliable measurement was their width (= Max Feret diameter, as defined below), which did not change once the profile was deemed to be symmetrical (Fig. 5A and B).

Initially, fibres were manually outlined using Adobe Photoshop CS6, and 16 parameters were measured by Image-Pro Plus 6.0 and ImageJ (Fig. 6). Since some parameters have similar characteristics and are highly correlated, only six parameters, such as Max Feret diameter, Min Feret diameter, Area, Perimeter, Convex Area and Convex Perimeter, were measured for our morphometric analysis of fibres in brachiopods (Fig. 6; Table 2; Głąb et al., 2015; Russ and Neal, 2015). Parameter definitions were modified from those available in Image-Pro Plus and ImageJ. We decided to use the measurements of Max Feret diameter and Min Feret diameter, which represent the caliper (feret) length, instead of Max and Min diameters because, in Image-Pro Plus 6.0, the diameter passes through the centroid of the

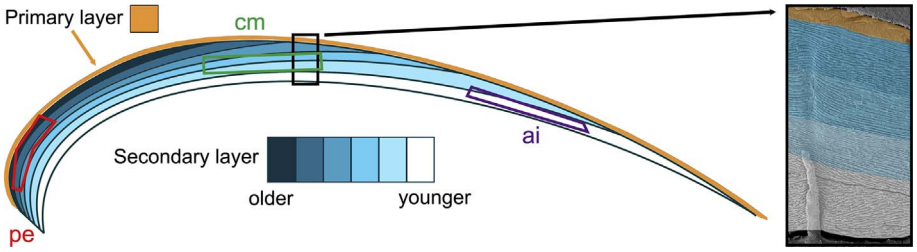

Fig. 4. Fibres were described and measured in different positions of the same shell: posterior, central and anterior from the umbo to the anterior margin and external, middle and internal along a vertical section through the secondary layer, following the direction of incremental growth of the shell. pe: posterior external; cm: central middle; ai: anterior internal (modified from Penman et al., 2013).

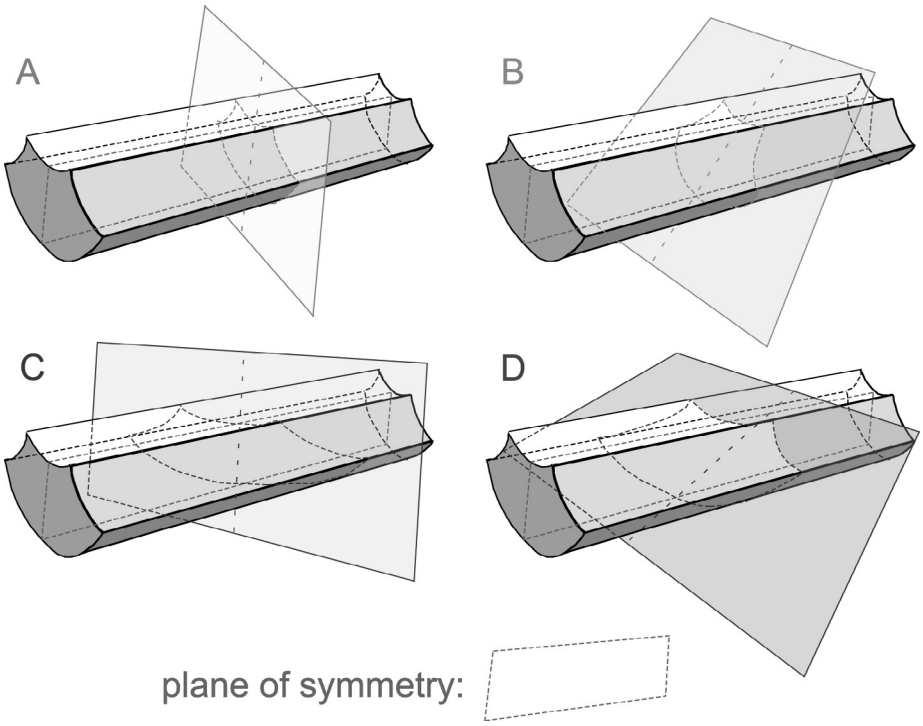

Fig. 5. Sections of fibres along different planes. A, section perpendicular to the plane of symmetry of the fibre; B, section perpendicular to the longitudinal axis of the fibre and tilted with respect to the plane of symmetry; C, section intersects obliquely the plane of symmetry; D, section is oblique and tilted with respect to the plane of symmetry.

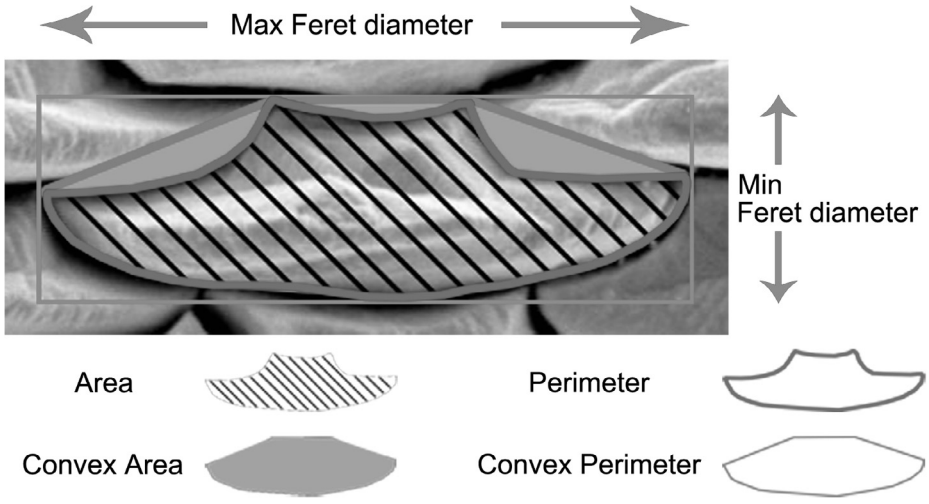

Fig. 6. Morphometric parameters used to define the size and shape of each fibre.

Table 2
Definitions of the six morphometric parameters used on the fibres of this study.

Parameters	Definitions
Max Feret diameter	Longest caliper length
Min Feret diameter	Smallest caliper length
Area	Area of the object
Perimeter	Length of the object's outline
Convex area	The area enclosed by the convex hull of the outer contour of the object
Convex perimeter	The perimeter of the convex hull of the object

object, so it was not a suitable descriptor of the shape of the fibres. Instead, the Max Feret diameter corresponds roughly to the width of an individual fibre, whereas the Min Feret diameter corresponds to its height (Fig. 6).

Furthermore, five shape descriptors were calculated, such as

Table 3
Procrustes ANOVA analysis of two groups of fibres. Group 1 comprises fibres judged to be symmetric. Group 2 comprises both symmetric and asymmetric fibres. Sums of squares (SS); mean squares (MS); Fluctuating asymmetry (ind:side) is used as error effect; P: *p*-values associated with the F distribution (after 999 permutations); side: side of each fibre representing the asymmetric component; Df: degrees of freedom.

Group 1	Df	SS	MS	F	Z-score	P (999 permutation)
individuals	29	0.31945	0.0110154	69.729	0.85173	0.830
side	1	0.00064	0.0006380	0.4039	0.31761	0.846
ind:side	29	0.04581	0.0015798			
Group 2	**Df**	**SS**	**MS**	**F**	**Z-score**	**P (999 permutation)**
individuals	39	0.41058	0.0105277	49.055	0.7872	0.936
side	1	0.01301	0.0130053	60.600	37.349	0.008
ind:side	39	0.08370	0.0021461			

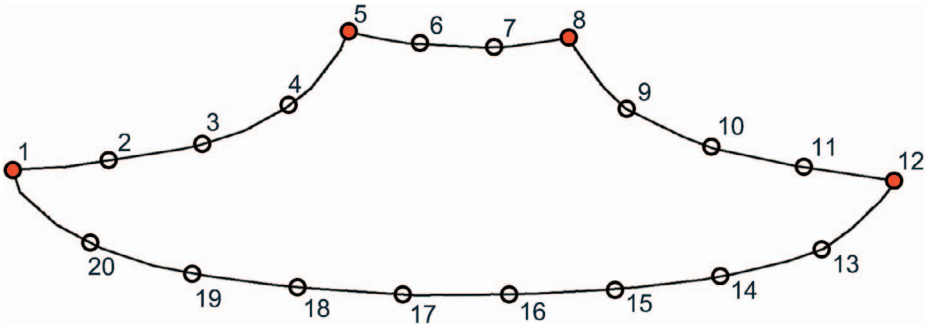

Fig. 7. Four landmarks (red circles) and sixteen semi-landmarks (open circles) digitized for each fibre. The semi-landmarks (2 to 4, 6 to 7, 9 to 11, and 13 to 20) are evenly distributed between the 4 landmarks (1, 5, 8 and 12). The marks (1 and 12, 2 and 11, 3 and 10, 4 and 9, 5 and 8, 6 and 7, 17 and 16, 18 and 15, 19 and 14, 20 and 13) are set as pairs based on the hypothetical axis of bilateral symmetry.

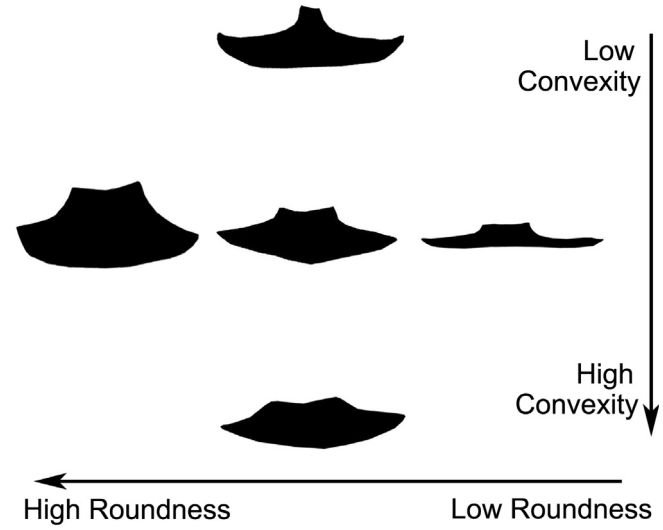

Fig. 8. Graphic visualization of the change in Roundness and Convexity of the fibres.

Formfactor (circularity, $4\pi \times$ Area/Perimeter^2), Roundness (4Area/$\pi \times$Max Feret diameter^2), Aspect Ratio (Max Feret diameter/Min Feret diameter), Convexity (Convex Perimeter/Perimeter), and Solidity (Area/Convex Area) with the six selected and measured parameters (Russ and Neal, 2015; Ye et al., 2017).

3.3. Data reliability analysis

To test the reliability of the visual selection process of symmetric fibres, two groups of data were compared using a geometric morphometric approach. Group 1 comprises 30 randomly selected fibres, that visually are considered symmetric, and Group 2 comprises both symmetric and asymmetric fibres (Table 3).

In cross section, 4 landmarks and 16 semi-landmarks were digitized for each fibre, following the scheme depicted in Fig. 7. The landmarks and semi-landmarks were digitized using TPSDIG 2.1. Following the procedure suggested by Mardia et al. (2000) and Klingenberg et al. (2002), pairs of landmarks were established based on geometric rules (Fig. 7). We partitioned the total shape of outlines between symmetric and asymmetric variants among fibres. Applying a two-factor ANOVA, we tested the effects of two sources of variability on the overall outline variation for the two datasets.

To perform the analyses we used the *bilat.symmetry* function, implemented in the package *geomorph* (Adams and Otarola-Castillo, 2013) for R 3.3.0 (R Core Team, 2016). Before starting the analysis of symmetry, semi-landmarks were aligned using the minimum bending energy criterion and a General Procrustes analysis to remove the effect of rotation, translation and size. Subsequently, the components of shape variation were decoupled among individuals, sides (directional asymmetry) and variation due to interaction among individual and side (fluctuating symmetry). Procrustes ANOVA was performed to assess the significance of each component in the two datasets (for further details see Klingenberg et al., 2002).

To work out the reliability of the measurements, the most

Table 4
Average values and standard deviations (in parenthesis) of Area (μm^2), Perimeter (μm), Max Feret diameter (μm), Roundness and Convexity of the fibres of ventral (V) and dorsal (D) valves. Results in bold are *p* values ranging from 0.05 to 0.001, and gray font background are *p*-values of < .001 (for more details see Ye et al., 2017).

Valve type	Number of measurements	Area	Perimeter	Max Feret diameter	Roundness	Convexity
V - *Liothyrella uva*	128	24.88 (7.95)	**24.89 (5.33)**	**10.87 (2.61)**	**0.279 (0.076)**	0.973 (0.012)
D - *Liothyrella uva*	102	26.89 (12.26)	**26.51 (6.74)**	**11.84 (3.33)**	**0.252 (0.074)**	0.975 (0.012)
V - *Gryphus vitreus*	93	26.34 (7.33)	27.65 (4.41)	12.65 (2.26)	0.217 (0.070)	**0.982 (0.009)**
D - *Gryphus vitreus*	184	19.72 (6.91)	23.95 (5.81)	10.92 (2.98)	0.226 (0.076)	**0.979 (0.010)**
V - *Liothyrella neozelanica*	134	25.04 (8.30)	26.59 (4.90)	12.07 (2.47)	**0.231 (0.083)**	0.981 (0.008)
D - *Liothyrella neozelanica*	147	24.04 (6.90)	27.28 (5.95)	12.57 (3.03)	**0.208 (0.071)**	0.982 (0.007)
V - *Calloria inconspicua*	40	**19.96 (5.08)**	**25.41 (4.40)**	**11.50 (2.24)**	**0.198 (0.046)**	0.970 (0.011)
D - *Calloria inconspicua*	30	**16.81 (5.38)**	**21.64 (4.34)**	**9.65 (2.28)**	**0.245 (0.086)**	0.973 (0.010)
V - *Magasella sanguinea*	81	29.08 (10.83)	26.65 (6.43)	11.88 (3.31)	0.279 (0.098)	0.981 (0.007)
D - *Magasella sanguinea*	54	27.67 (11.45)	25.71 (6.38)	11.46 (3.15)	0.279 (0.092)	0.981 (0.008)
V - *Notosaria nigricans*	105	35.06 (15.89)	32.53 (9.94)	15.01 (4.96)	0.212 (0.071)	0.982 (0.010)
D - *Notosaria nigricans*	99	39.44 (16.19)	32.45 (9.64)	14.61 (4.88)	0.258 (0.097)	0.980 (0.009)
Ventral - all 6 species	581	**27.29 (10.90)**	**27.42 (6.85)**	12.38 (3.47)	0.240 (0.083)	0.979 (0.011)
Dorsal - all 6 species	616	**25.66 (12.28)**	**26.78 (7.37)**	12.04 (3.66)	0.237 (0.083)	0.979 (0.010)

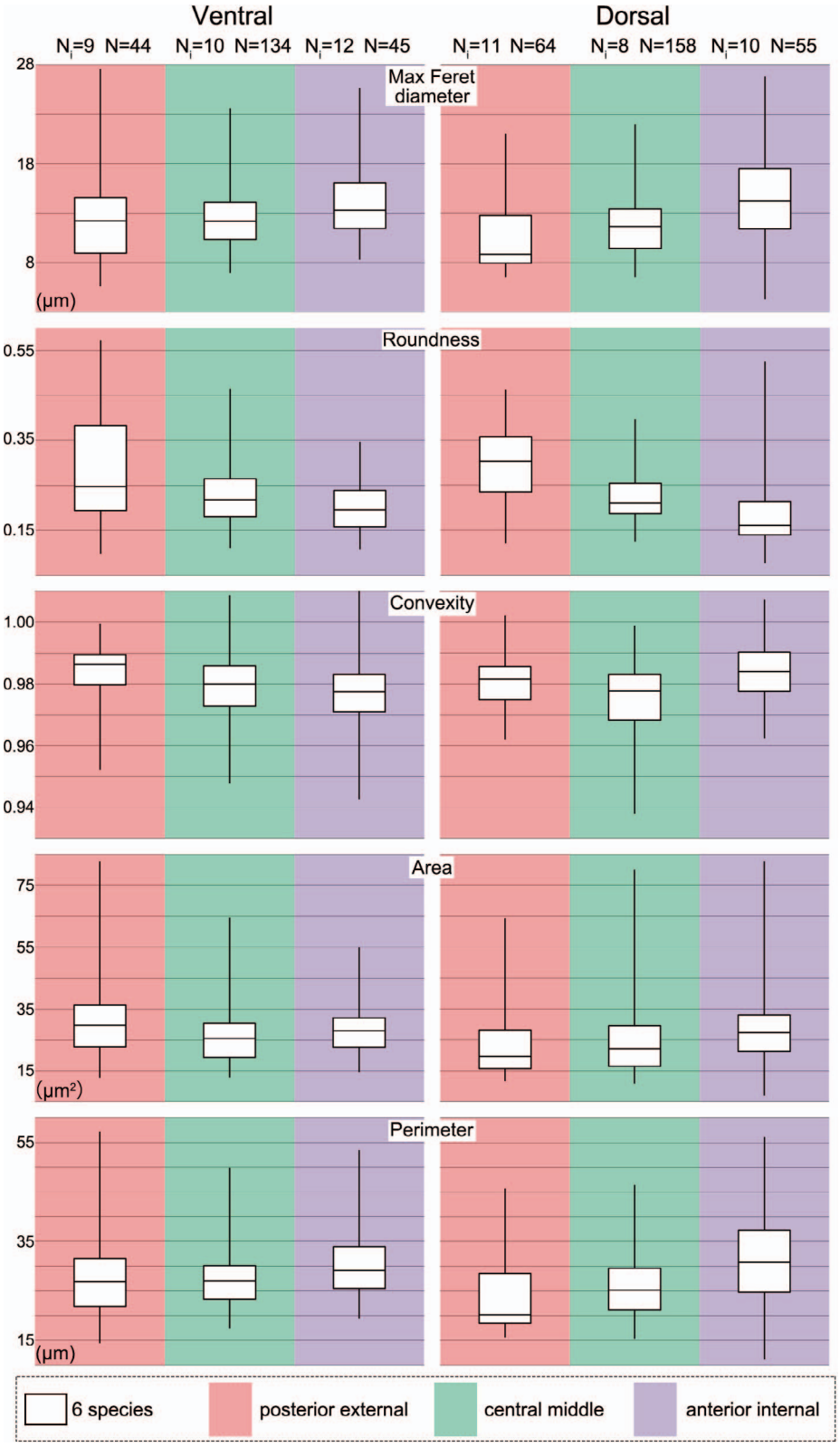

Fig. 9. Box plots showing the difference in fibre sizes and shapes of all six species at different ontogenetic stages. The bottom/top of the box and the band inside the box are the first/third quartiles and the median of the data respectively; ends of the whiskers represent the minimum and maximum of results. N_i: number of individuals; N: number of measurements.

significant parameters (Area, Perimeter, Max Feret diameter, Convex Area) were tested in Excel for their probability density (cf. Duller, 2008). The assumption of normality was tested through the shapes of data distributions and the frequency distribution within the data range. Independent-sample *t*-tests were performed using SPSS Statistics (IBM Version 22.0. Armonk, NY). A *p*-value ≤ .05 is considered significant and a *p*-value ≤ .001 is considered highly significant.

4. Results

4.1. Data reliability and statistical analyses

For Group 1 results, the Procrustes ANOVA shows that among fibres the symmetric and asymmetric variations have similar *p*-values (.83–.85), which are not significantly different. For Group 2 results, the

Table 5
Measurements of the structural units (fibres) in different shell positions (v: ventral, d: dorsal; pe: posterior external, cm: central middle; ai: anterior interior). Average values and standard deviations (in parentheses) of the data for Area, Perimeter, Max Feret diameter, Roundness and Convexity. LU: *L. uva*; GV: *G. vitreus*; LN: *L. neozelanica*; NN: *N. nigricans*.

Valve and position	Number of measurements	Area	Perimeter	Max Feret diameter	Roundness	Convexity
LUvpe	11	25.02 (10.19)	23.21 (7.27)	9.97 (3.63)	0.357 (0.125)	0.979 (0.013)
LUvcm	36	22.23 (6.78)	24.58 (4.56)	10.75 (2.23)	0.249 (0.052)	0.968 (0.010)
LUvai	13	24.74 (7.39)	26.15 (5.07)	11.66 (2.41)	0.236 (0.048)	0.973 (0.010)
LUdpe	13	20.10 (3.49)	20.19 (2.35)	8.63 (1.28)	0.353 (0.073)	0.980 (0.012)
LUdcm	35	32.85 (16.42)	29.93 (7.24)	13.45 (3.60)	0.229 (0.052)	0.972 (0.013)
LUdai	7	24.86 (10.89)	26.36 (8.12)	11.99 (3.73)	0.221 (0.043)	0.980 (0.010)
GVvpe	13	34.15 (6.07)	30.06 (4.13)	13.71 (2.36)	0.249 (0.096)	0.990 (0.005)
GVvcm	22	24.37 (5.76)	27.09 (3.47)	12.45 (1.69)	0.202 (0.039)	0.979 (0.007)
GVvai	4	26.09 (3.37)	28.55 (2.79)	13.27 (1.28)	0.192 (0.037)	0.987 (0.006)
GVdpe	16	16.25 (2.79)	18.35 (1.39)	7.91 (0.74)	0.335 (0.064)	0.980 (0.006)
GVdcm	40	16.70 (3.30)	22.16 (2.79)	9.98 (1.46)	0.219 (0.049)	0.972 (0.012)
GVdai	12	31.65 (9.80)	34.32 (6.46)	16.40 (3.16)	0.150 (0.026)	0.992 (0.007)
LNvpe	9	25.04 (7.15)	23.39 (3.49)	10.15 (1.80)	0.320 (0.094)	0.980 (0.008)
LNvcm	25	23.64 (11.35)	27.00 (4.82)	12.44 (2.18)	0.194 (0.058)	0.982 (0.009)
LNvai	14	28.20 (5.56)	29.50 (4.33)	13.52 (2.26)	0.203 (0.048)	0.977 (0.007)
LNdpe	23	23.95 (9.66)	25.64 (8.23)	11.72 (4.18)	0.248 (0.086)	0.982 (0.006)
LNdcm	27	24.37 (6.34)	27.94 (5.18)	12.96 (2.53)	0.189 (0.039)	0.982 (0.006)
LNdai	24	25.91 (7.01)	30.44 (5.39)	14.19 (2.76)	0.175 (0.065)	0.982 (0.008)
NNvpe	6	55.75 (21.18)	44.74 (13.35)	21.00 (6.90)	0.181 (0.083)	0.987 (0.008)
NNvcm	22	31.50 (7.46)	30.98 (6.47)	14.35 (3.21)	0.203 (0.045)	0.985 (0.008)
NNvai	9	34.93 (12.51)	36.08 (8.91)	16.80 (4.43)	0.162 (0.045)	0.979 (0.020)
NNdpe	9	46.87 (15.32)	34.64 (6.33)	15.43 (3.11)	0.254 (0.075)	0.974 (0.009)
NNdcm	17	35.87 (11.16)	31.31 (5.40)	14.18 (2.58)	0.226 (0.035)	0.979 (0.009)
NNdai	9	43.51 (20.32)	38.23 (11.86)	17.83 (5.91)	0.189 (0.081)	0.982 (0.006)
vpe	44	31.79 (14.46)	28.22 (9.69)	12.63 (5.01)	0.292 (0.125)	0.984 (0.010)
vcm	134	26.66 (9.86)	27.44 (5.92)	12.44 (2.98)	0.227 (0.065)	0.979 (0.011)
vai	45	28.89 (9.04)	30.21 (6.71)	13.83 (3.39)	0.201 (0.052)	0.977 (0.012)
dpe	64	24.80 (12.77)	23.89 (7.67)	10.58 (3.77)	0.299 (0.089)	0.980 (0.008)
dcm	158	25.08 (12.13)	26.41 (6.41)	11.97 (3.13)	0.223 (0.056)	0.976 (0.011)
dai	43	28.22 (14.32)	30.39 (9.17)	14.10 (4.52)	0.184 (0.076)	0.984 (0.009)

asymmetric component (Side) of the fibres shows a significant *p*-value (.008). Thus, in the selected fibre set, shape variability is not affected by asymmetry. In contrast, the second dataset is significantly affected by asymmetry, confirming that the visual selection process is reliable in distinguishing between types of fibres.

Six parameters: Area, Perimeter, Max Feret diameter, Min Feret diameter, Convex Perimeter, Convex Area – involving 1197 fibre measurements – were tested by Excel for their probability distribution (Figs. 1–3 in Ye et al., 2017). The results show that the Max Feret diameter is the most reliable morphometric measure – supporting the assumption of the morphometric analysis (paragraph 3.2) – and Roundness and Convexity are the best morphometric descriptors of shape variation (Fig. 8).

4.2. Shape and size of fibres: Dorsal vs ventral valves

For comparison of shape and size, we made 1197 measurements on six recent brachiopod species, representing 581 measurements on fibres from ventral valves and 616 measurements on fibres from dorsal valves (Table 4). In the *t*-test results for all six species, the *p*-values between dorsal and ventral fibres of Max Feret diameter (.116), Roundness (.470) and Convexity (.869) are greater than .05 and so reveal no statistically significant difference between them. The *p*-values for difference relative to Area (.019) and Perimeter (.049) are significant ($p \leq .05$), but this may be related to the fact that the distribution curves are skewed (Figs. 1–3 in Ye et al., 2017). This is also evident when comparing fibres from corresponding positions in both valves measured in the anterior internal part of the dorsal valve with those measured in the anterior internal part of the ventral valve ($p > .05$). Overall, there is no significant difference in the size and shape of fibres between ventral and dorsal valves.

C. inconspicua and *G. vitreus* show a highly significant difference in Max Feret diameter ($p \leq .001$) and a significant difference in Roundness ($p \leq .05$) between dorsal and ventral valves. *L. uva* exhibits a significant difference ($p \leq .05$) in size and Roundness. *L. neozelanica* and *N. nigricans* have significant and highly significant differences only in the Roundness of the fibres of the two valves, respectively, whereas the other species show no significant difference in these morphometric parameters between the two valves.

4.3. Shape and size of fibres: Ontogenetic variation

Fibres were measured at specific locations in the shell along its growth axis (Fig. 4), allowing us to check if there is an ontogenetic trend in the size and shape of the fibres. Overall, when we compare morphology and size of fibres along the growth direction from the posterior external part to the anterior internal part of each valve, the fibres become progressively larger, wider, less round (lower Roundness), and flatter (higher Aspect ratio) with age (Fig. 9; Table 5). In addition, fibres of the ventral valves become also less convex with increasing age. Significant to highly significant ($p \leq .05$ and $p \leq .001$) differences in the Perimeter, Max Feret diameter, Roundness and Convexity of the fibres from the different regions of the shell were observed along the growth transect in the dorsal valve of all species. Overall, measurements of fibres from the mid-section (vcm and dcm) of the shells (dorsal and ventral) are most consistent for Max Feret diameter and Roundness (Table 5).

The Max Feret diameter of fibres from the posterior to the anterior increased by 11% in the ventral and by 33% in the dorsal valves, and the average decrease in Roundness of the anterior internal fibres is 31% in the ventral and 39% in the dorsal valves (Table 5).

The fibres of the dorsal valve of *G. vitreus* show a highly significant change in size and shape with age, whereas those of *L. neozelanica* show a significant difference in Max Feret diameter and Roundness. In contrast, the *t*-test of the overall ventral valve data show a significant difference ($p \leq .05$) only for the Roundness and Convexity of the fibres.

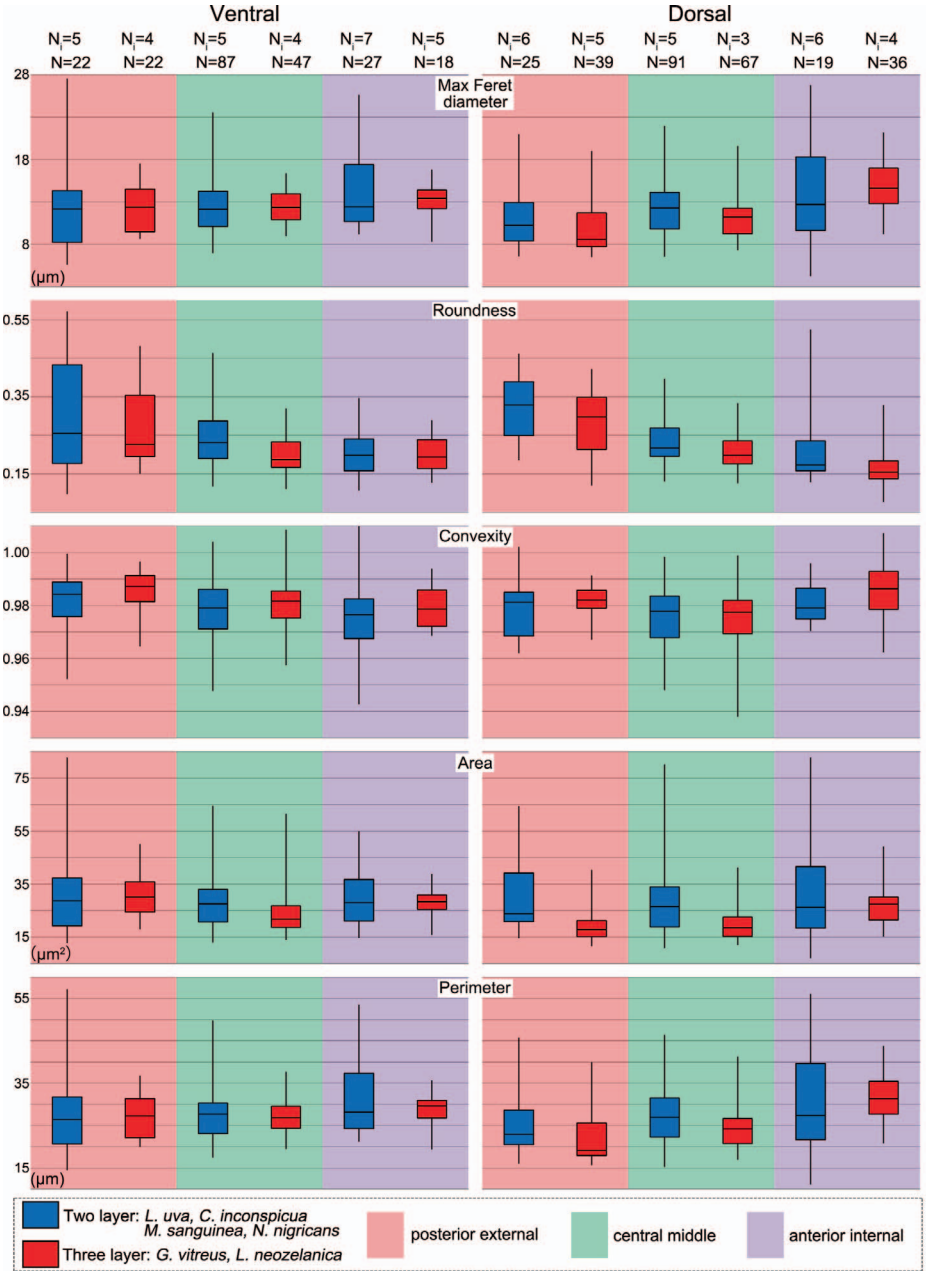

Fig. 10. Box plots showing the difference in fibre sizes and shapes of species with two-layer shells (*L. uva*, *C. inconspicua*, *M. sanguinea* and *N. nigricans*) and species with three-layer shells (*L. neozelanica* and *G. vitreus*) in different parts of the ventral and dorsal valves. The bottom/top of the box and the band inside the box are the first/third quartiles and the median of the data respectively; ends of the whiskers represent the minimum and maximum of the data. N_i: number of individuals; N: number of measurements.

This result may be affected by the unusual fibre distribution in *G. vitreus* and *N. nigricans*, where they are variable in size from the posterior external part of the ventral valve. Also, posteriorly, fibres are larger than those of the central middle part and anterior internal part (Table 5), but this difference is not significant ($p > .05$). At the species level, *L. neozelanica* shows a highly significant change in fibre Perimeter, Max Feret diameter and Roundness with age.

4.4. Shape and size of fibres: two-layer vs three-layer shells

The size and shape of the fibres were compared in species with different shell layer sequences, such as those with two layers (Group 1: *L. uva, C. inconspicua, M. sanguinea* and *N. nigricans*) to those with three layers (Group 2: *G. vitreus* and *L. neozelanica*) (Fig. 10). The differences in size and shape are significant to highly significant ($p \leq .05$ and $p \leq .001$) for the dorsal valve fibres of the two groups. Fibres in the three-layer brachiopods are less round and larger in the anterior internal part, but smaller in the central middle and posterior external parts with respect to those of the two-layer shells (Fig. 10). In the ventral valve, the differences in Area, Roundness and Convexity are highly significant between the two groups ($p \leq .001$); however the differences in Area should be considered with caution as they may be affected by the orientation of the section (see Fig. 5). In the central middle part of the shell, the fibres of the three-layer brachiopods are less round and more convex. Size and shape of fibres in the three-layer brachiopods are always significant to highly significantly different in the dorsal valves, but not in the ventral valves, except for the posterior external part ($p < .05$) (Table 5).

EBSD band contrast images show a striking difference in fibre dimension and morphology between the three-layer shells of *G. vitreus* and *L. neozelanica*. Fibres in cross-section are large and rounded in *L. neozelanica*, whereas they are highly elongated and flat in *G. vitreus* (Fig. 11). The microstructure of *G. vitreus* is dominated by a thick columnar layer, whereas in *L. neozelanica* not only is the columnar layer thinner, but it also shows frequent intercalation with the fibrous layer.

Comparing species with different shell layer sequences (two-layer:

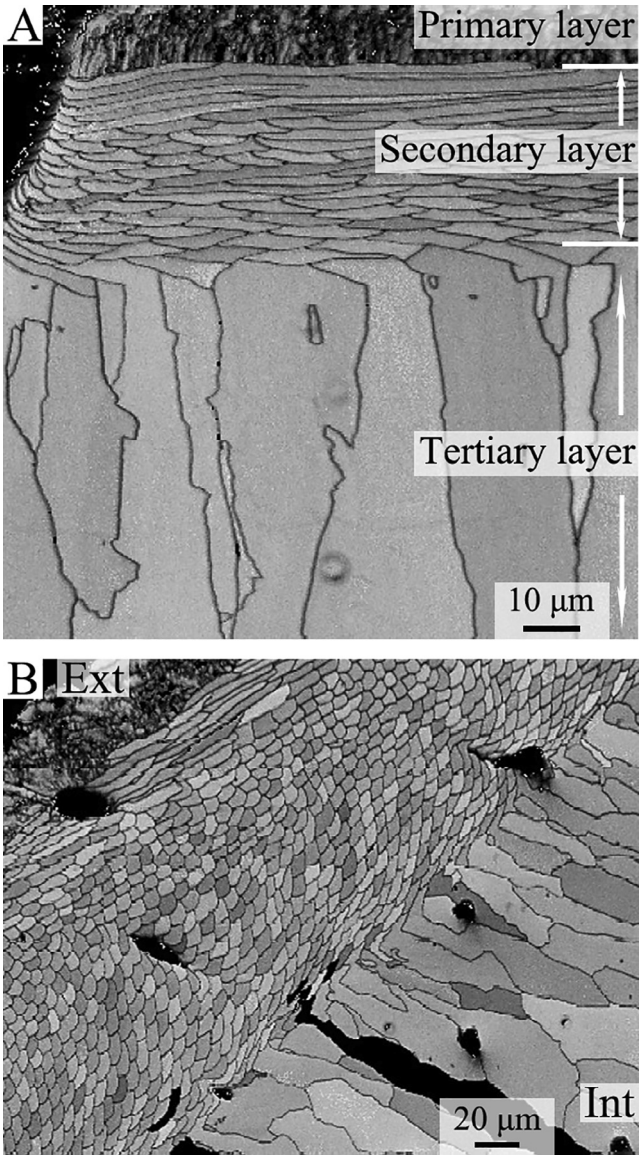

Fig. 11. EBSD band contrast images visualizing the difference in microstructure of the studied three-layer shell specimens. A, *G. vitreus*; B, *L. neozelanica*. Ext: external, Int: internal.

N. nigricans, C. inconspicua, M. sanguinea; three-layer: *L. neozelanica*) from the same locality (Doubtful Sound, New Zealand), the size of the ventral fibres and the Area, Roundness, and Convexity of the dorsal fibres are significant to highly significantly different ($p \leq .05$ and $p \leq .001$). Overall, the fibres of two-layer brachiopods are larger than of their three-layer counterparts.

4.5. Shape and size of fibres: Environment

To estimate fibre variation among different localities, we compared the New Zealand fauna (NZ) against the Mediterranean (Med) and the Antarctica ones (Ant). However, to exclude effects related to different shell sequence (see paragraph 4.4) we treated the three-layer shell of *L. neozelanica* from New Zealand as a separate unit (LN) (Fig. 12; Table 4). The three-layer brachiopod *G. vitreus* represents the Mediterranean environment. The New Zealand and Mediterranean localities are characterized by different water depths, and salinity, but similar temperatures and hydrodynamic energy (Table 1), with the first recessed into a fjord whereas the second is in relatively deep water. The Antarctic localities stand out by their lower seawater temperatures and lower carbonate saturation state (Watson et al., 2012; Takahashi et al., 2014).

L. uva from Antarctica differs from the other brachiopods from New Zealand and the Mediterranean by its smaller-sized, lower Convexity and higher Roundness fibres (Fig. 12). These differences are always significant to highly significant ($p \leq .05$ and $p \leq .001$) in the ventral valve. The differences in Max Feret diameter of the dorsal fibres between *L. uva* and *L. neozelanica* are not significant ($p > .05$).

Comparing the Mediterranean and New Zealand species, there is a significant difference in the Area, Perimeter and Convexity of the fibres of the ventral valves ($p = .001$ in Area, $p = .039$ in Perimeter; $p = .033$ in Convexity); the largest fibres are those of the New Zealand two-layer species, the smallest are those of the three-layer brachiopod *L. neozelanica* (Fig. 12). In the dorsal valve, the differences are significant to highly significant for nearly all morphometric parameters ($p \leq .05$ and $p \leq .001$) and the largest fibres are those in the New Zealand species (Fig. 12).

4.6. Shape and size of fibres: The Liothyrella species case

We analysed two species of the same genus living in different environmental conditions, to check for interspecific variability and environmental control on the size and shape of the fibres. Overall, fibres at the same ontogenetic stage of the two species are smaller, narrower, rounder, less flat and less convex in *L. uva* than those in *L. neozelanica* (Fig. 13; Table 5). However, in the central middle part of the dorsal valve only, the fibres of *L. uva* are larger in Area and have a higher Max Feret diameter than those in *L. neozelanica*. The size and shape of the fibres are highly significantly different in the ventral valves of the two species ($p \leq .001$ in Max Feret diameter, Roundness and Convexity); in the dorsal valves only the shape is highly significantly different ($p \leq .001$ in Roundness and Convexity).

EBSD band contrast images show that the shell of *L. uva* is formed of smaller fibres compared to the other brachiopod species.

To investigate the nanostructure of the two species at a finer scale, TEM observations were undertaken on the primary and secondary layers of *L. uva* and on secondary and tertiary layers of *L. neozelanica* (Figs. 14–16). The two species show similar secondary layer structure. Fibres in transverse section (Fig. 14A) appear as single crystals (Fig. 14B), are several micrometres long and 3–5 µm thick, with the *c*-axis approximately in the plane of the section and parallel to the shortest dimension. The most eye-catching feature is the large amount of round inclusions with dimensions up to a few hundred nanometres, containing amorphous material and in some cases a solid crystalline precipitate (Fig. 14C), locally forming ribbons (Fig. 14D) that are interconnected by dislocations (Fig. 14E). Compositional profiles of the inclusions show that they are enriched in either S or Si, with respect to the host calcite (Fig. 15). The single crystalline nature of fibres, the crystallographic c-axis orientation with respect to the external surface of the valve and to the morphology of the fibre are consistent with the results of Goetz et al. (2009).

The primary layer shows comparatively smaller single crystals (less than one micron wide and 1–2 µm long), elongated along the *c*-axis (Fig. 16A). Also, the primary layer crystals contain inclusions, although in smaller amount. Inclusions are smaller (tens of nanometers) than those occurring in the secondary layer, and often characterized by polygonal borders similar to the rhombohedral cleavage of calcite (Fig. 16B). Inclusions sometimes align along grain borders and do not always contain a solid crystalline precipitate. The tertiary layer of *L. neozelanica* is formed by large single crystals (several microns) (Fig. 16C) with few sporadic inclusions. Adjoining crystals seem related by a $n60^\circ$ rotation around the *c*-axis, which lies on the thin section plane (Fig. 16D–F). EBSD measurements clearly resolve the characteristics of the crystals of the tertiary layer (Fig. 11).

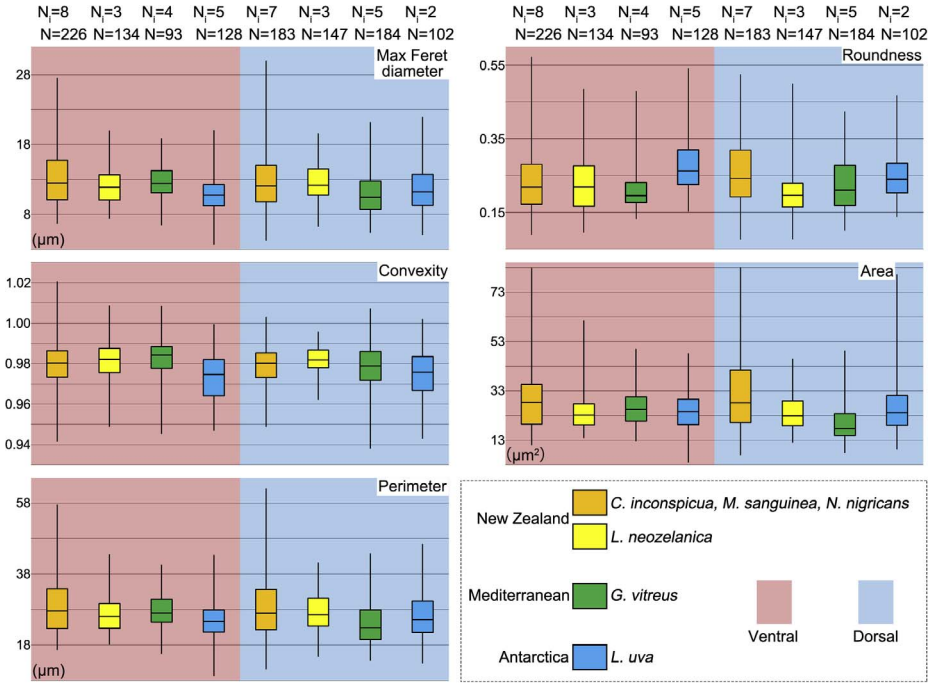

Fig. 12. Box plots showing the differences in fibre sizes and shapes among species with two-layer shells from New Zealand (*C. inconspicua, M. sanguinea* and *N. nigricans*), three-layer shells from New Zealand (*L. neozelanica*), three-layer shells from the Mediterranean (*G. vitreus*), and two-layer shells from Antarctica (*L. uva*), of their ventral and dorsal valves. The bottom/top of the box and the band inside the box are the first/third quartiles and the median of the data respectively; ends of the whiskers represent the minimum and maximum of the results. N_i: number of individuals; N: number of measurements.

5. Discussion

Fibres of the secondary layer change their morphological orientation during growth, so that a single longitudinal section of a shell will not cut all fibres along the same section (Williams, 1966, 1968, 1997; Schmahl et al., 2004, 2012; Goetz et al., 2009; Gaspard and Nouet, 2016; Garbelli, 2017). The method followed in this research selected sections that represented perpendicular cuts of the fibres and recorded their actual size. It is appropriate to discuss further the fibre morphometric variation in relation to biotic factors and environmental control.

5.1. Fibres, ontogeny and shell fabric

Morphometric analysis of fibres in dorsal and ventral valves has important implications for the geochemical proxies and the information stored by the valves, as it is still controversial whether the two valves are formed in equilibrium with ambient seawater. Curry and Fallick (2002) reported different $\delta^{18}O$ values from ventral and dorsal valves of the same brachiopod specimen. However, recent studies found no significant difference in the geochemistry (trace chemistry and stable isotopes) between dorsal and ventral valves (Parkinson et al., 2005; Brand et al., 2015).

Based on no difference in fibre shape and size between dorsal and ventral valves, no difference in the geochemical composition of the secondary layer should be expected between the two valves. However, individually, a few species show some differences in fibre morphometrics between valves. Griesshaber et al. (2007) demonstrated that the dorsal and ventral valves of two recent species (*Terebratalia transversa* and *Megerlia truncata*) have different microstructural features. Therefore, there is a possibility in difference in fibre morphometrics at the species-specific level (i.e. in some species only).

Microstructural changes may occur within different shell layers and even in single shell layers (Grossman et al., 1996; Auclair et al., 2003; Griesshaber et al., 2005, 2007; Garbelli, 2017). Our results show that the fibres change in size and shape passing from the posterior external, to the central middle, and finally to the anterior internal part. As the posterior external part is produced first, whereas the anterior internal shell is produced last, there is an ontogenetic trend in the size and shape of the fibres, with the largest, widest and flattest fibres being produced at the last and mature ontogenetic stages.

Variation of fibre size and shape in the growth direction may be related to the geochemical signal recorded in different parts of the shell (Griesshaber et al., 2007; Cusack et al., 2007; Garbelli et al., 2012, 2014). Yamamoto et al. (2011, 2013) reported oxygen isotope variations in different shell portions and related this to variable growth rates. Other researchers found that the inner part of the shell (inner part of secondary and tertiary layers) are in equilibrium with seawater and are the best biogenic materials for geochemical analyses (e.g., Grossman et al., 1996; Parkinson et al., 2005; Garbelli et al., 2012; Cusack and Huerta, 2012; Rollion-Bard et al., 2016). Here, we have shown that these inner (and anterior) fibres – produced at the later ontogenetic stage – are generally large, wide, and flat. Therefore, there is a relationship between the capacity to record the geochemical signal and fibre morphometrics, which may depend on ontogeny and growth rate, which in brachiopod decreases with age (Peck, 2001).

When comparing groups of species with two-layers against three-layer shells, the pattern is not straightforward. So, we conclude from this that the shell layer sequence is not the determinant factor in controlling the size and shape of the fibres of the secondary layer.

5.2. Shell organic content

In a previous study to assess the organic content of the shells of *L. uva* and *L. neozelanica,* using an ash free dry mass determined by ignition loss, the means were 3.38% and 1.87% respectively (Peck and Edwards, 1996). Our study explains how these differences are related to the microstructures observed because the size of fibres shows a relationship with organic matter content of the shell whereby the larger the calcite fibres, the smaller the amount of organic membrane matter coating the fibres in the same shell volume (cf. Garbelli et al., 2017). The shape of the fibres, in particular their convexity, also plays a role, because a lower convexity means a more intricate outline allowing for enhanced development of organic membranes coating the fibres (cf. Fig. 8).

TEM observations of the secondary layer at the nanoscale show that there are no differences at this scale between the fibres of *L. uva* and those of *L. neozelanica*, both being characterized by high density of inclusions. Thus, the differential amount of organic matter stored in

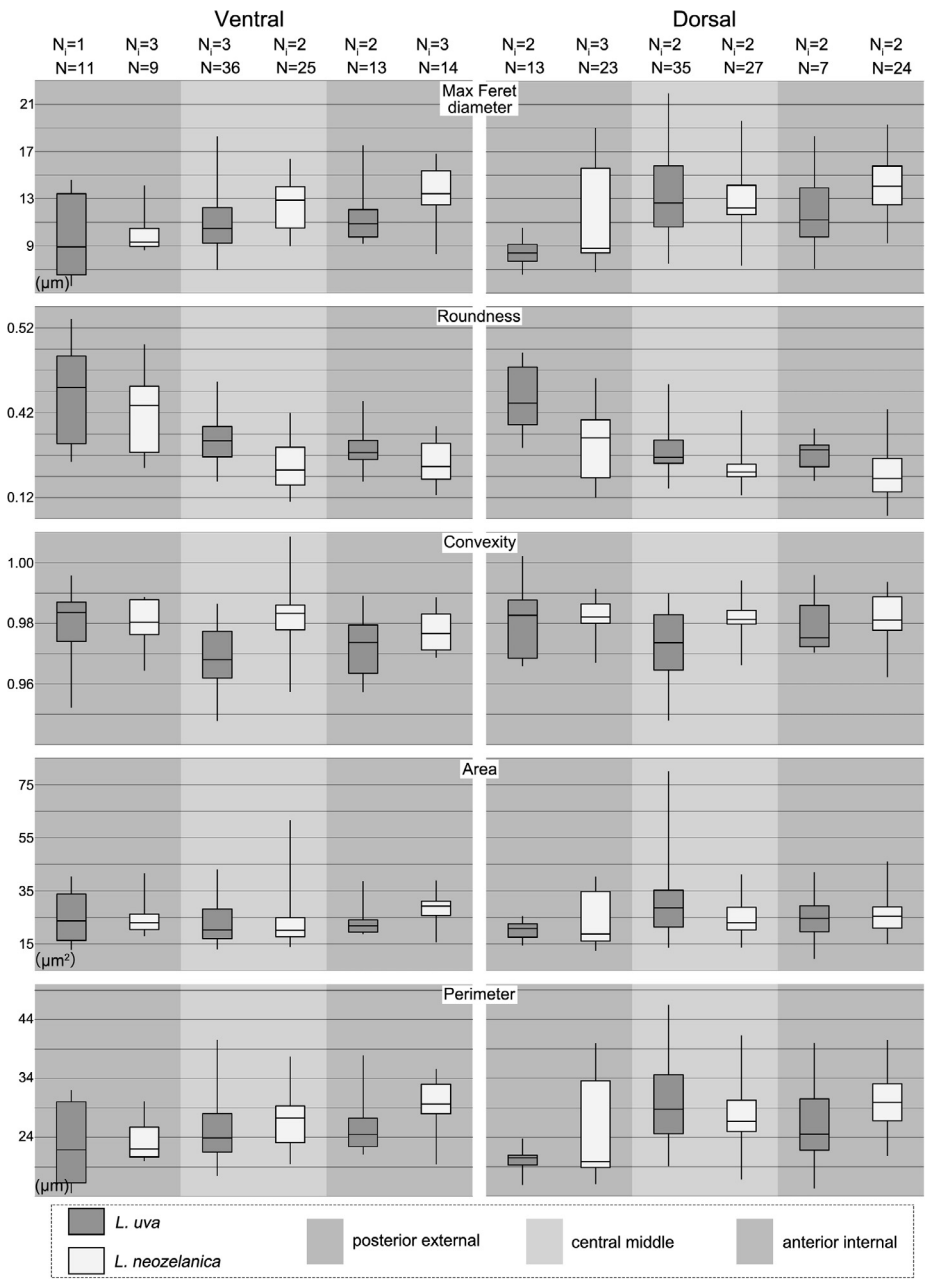

Fig. 13. Box plots showing the difference in fibre sizes and shapes of *L. uva* (blue) and *L. neozelanica* (yellow). The bottom/top of the box and the band inside the box are the first/third quartiles and the median of the data respectively; ends of the whiskers represent the minimum and maximum of the data. N_I: number of individuals; N: number of measurements.

their respective shells should be related to the organic matter membranes among the fibres, rather than their intra-crystalline inclusions.

Our results on secondary layer fibres of generally being larger, wider, flatter and less round interiorly and anteriorly suggest that portions produced at this later ontogenetic stage must be associated with lower organic matter contents. This may be related to growth rate, but also to the energy balance of the organism (Peck, 2001). It has been suggested that the metabolic cost for precipitating $CaCO_3$ is lower than the one required for the secretion of organic membranes in the biomineral (Palmer, 1992). Thus, it may be possible that brachiopods with age shift to a slower, energy-conserving organic-poor growth process. In addition, brachiopods from cold water environments include more organic matter with their smaller fibres than counterparts from temperate regimes with larger fibres.

5.3. Shell hardness and predation

Fibres measured in the posterior external part of the shell of *G. vitreus* (Terebratulida) and *N. nigricans* (Rhynchonellida) are larger and less round in the ventral than in the dorsal valve.

Fibre size differences in the secondary layer may reflect changes in mechanical properties that control shell bending, attachment to hard substrate, mobility or resistance to predation. According to Pérez-Huerta et al. (2007) and Goetz et al. (2009), hardness decreases from the outside to the inside of the shell. Pérez-Huerta et al. (2007) found that the posterior part of the shell is softer and less stiff than the central and anterior regions. Goetz et al. (2009) showed that the fibrous layer is harder when the fibres are thin and randomly stacked. In the case of *G. vitreus* and *N. nigricans*, the fibres being larger and more uniformly oriented may indicate a softer and less stiff ventral posterior region. However, the larger the fibres the thicker the secondary layer produced in a certain amount of time, and shell thickness is one of the most effective defence mechanism against durophagous predation (Zuschin et al., 2003). Larger fibres allow brachiopods to increase shell thickness more rapidly, and ensure defence against predation. This may be a clear survival advantage during early stages of growth, characterized by

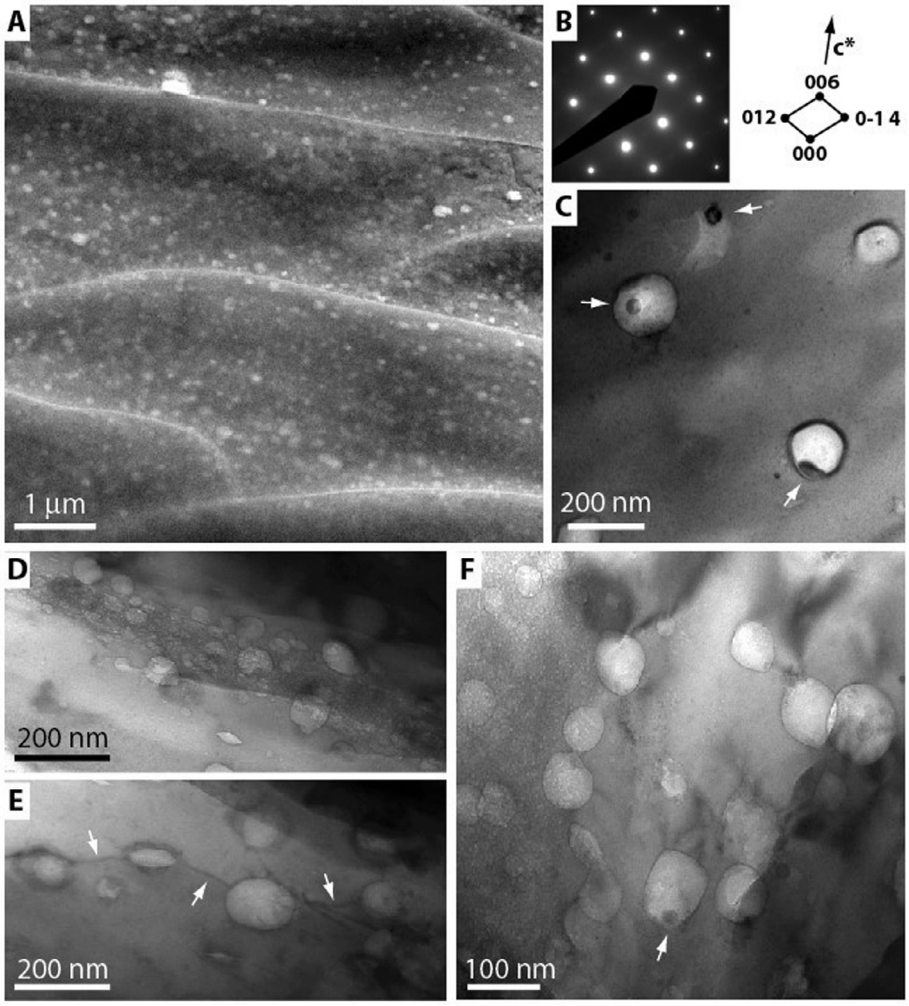

Fig. 14. TEM images of the secondary layer of *L. neozelanica* (A-E) and *L. uva* (F). A, low magnification image showing fibres in cross-section embedding numerous inclusions (brighter areas); B, diffraction pattern with spot indexing (right) showing the c-axis orientation with respect to the fibre section (beam incidence ⟨100⟩); C, bright field image showing crystalline precipitates (arrows) within the inclusions; D, concentration of round inclusions forming a ribbon; E, inclusions interconnected by dislocations (arrows); F, round inclusions similar to those observed in *L. neozelanica*; in some cases showing crystalline precipitates (arrow).

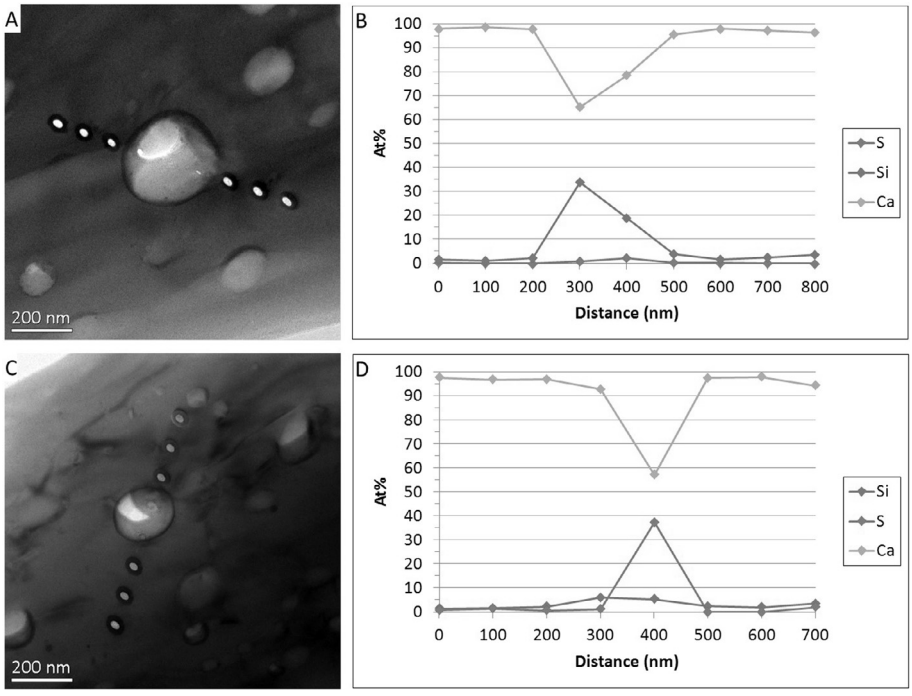

Fig. 15. Compositional profiles across round inclusions with a glassy interior (*L. neozelanica*, secondary layer) showing enrichment in silicon (A-B) and sulphur (C-D), with respect to the surrounding calcite matrix (the bright spots with dark halo in A and C correspond to the point analyses graphed in B and D, respectively).

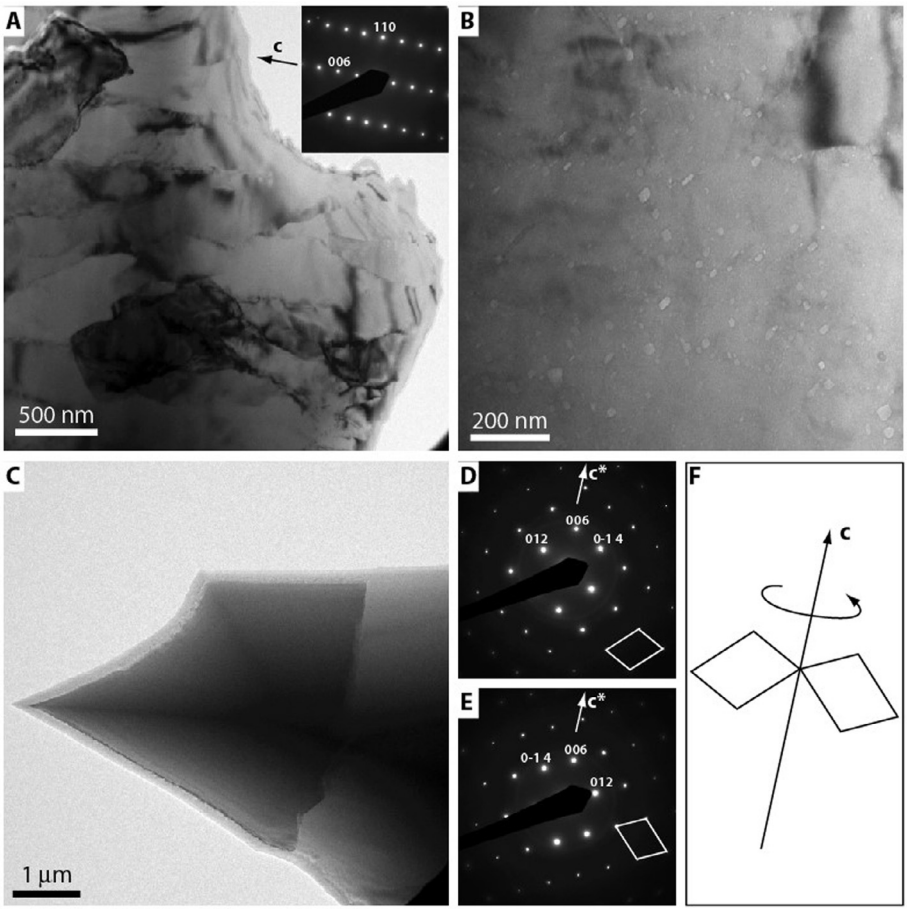

Fig. 16. A-B, Primary layer of *L. uva* and C-F, tertiary layer of *L. neozelanica*. A, TEM bright field image showing micrometre-sized calcite grains and related single crystal diffraction pattern (inset). The diffraction pattern is taken along ⟨1-1 0⟩ and the *c*-axis lies approximately on the thin section plane; B, bright field image with the calcite grains out of contrast to highlight the small inclusions with rhombohedral facets; C, two adjoining calcite grains (only a portion of them is shown) related by a *n* 60° rotation around the *c*-axis, as inferred from the diffraction patters in D and E (beam incidence ⟨100⟩), which refer each to individual grains, and the explaining scheme in F.

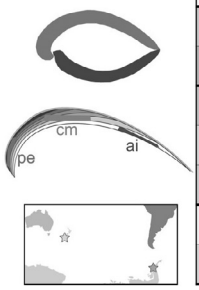

	Max Feret diameter	Roundness	Convexity
Ventral valve Dorsal valve	Inconclusive change	Inconclusive change	Inconclusive change
Posterior external	narrow	round	Inconclusive change
Central middle	median	median	
Anterior internal	wide	flat	
Temperate: *L. neozelanica*	wide	flat	simple
Antarctica: *L. uva*	narrow	round	intricate

Fig. 17. Overview of the main results of this research showing change of fibre size and shape with age and in different environments.

faster, but a variable growth rate (Rosenberg et al., 1988; Curry and Fallick, 2002).

Delance and Emig (2004) showed that in the Mediterranean *G. vitreus,* predation drillholes are mostly located on the posterior and thickest part of the ventral valve. The same was observed by Harper et al. (2011) for *N. nigricans*. Delance and Emig (2004) concluded that *G. vitreus* does not exhibit any antipredatory adaptations and that drilling predation pressure is generally low in this species. Instead, they suggested that crushing predation would be more important, and, in their experiments, the most resistant part to this kind of predation would be the posterior and thickest region of the shell.

New Zealand *L. neozelanica*, which has a three-layer shell sequence similar to that of *G. vitreus*, does not have larger fibres in the posterior region. Interestingly, Harper and Peck (2016) have shown that *L. neozelanica* has lower rates of repair than co-occurring brachiopods as it suffers lower predation pressure. Consequently, larger fibres posteriorly may represent a survival strategy to rapidly increase shell thickness against shell-breaking predation.

5.4. Environmental control

It is quite reasonable to assume that environmental conditions may, in part, control the microstructural variation observed in fibres of the brachiopods from the Mediterranean Sea, a fjord of New Zealand and the bays of Antarctica. When comparing species living in different environmental settings, *L. uva*, from cold (± 2 °C) and less saturated seawater of Antarctica, faces the greatest challenge compared to the others from New Zealand and the Mediterranean. The brachiopods, particularly the two-layer species, from New Zealand have the largest and widest fibres, and they seem to be different from the Mediterranean species *G. vitreus*. However, the two settings have similar temperatures and rather low hydrodynamic energy, so other factors may control their different microstructures, such as salinity and/or carbonate saturation.

Seawater carbonate saturation for the Mediterranean Sea of 4.7 Ω (Alvarez et al., 2014) and 4.0 for New Zealand (Takahashi et al., 2014) suggests that seawater in the Mediterranean Sea with its higher saturation and salinity, may be an additional factor for the less organic

rich shell microstructure of *G. vitreus*.

The effect of temperature and seawater carbonate saturation state is even more pronounced when we consider the size and shape differential of fibres in the two species of the same genus, *L. uva* and *L. neozelanica,* from different environmental settings. The Antarctic and New Zealand localities have similar salinity, but significantly different temperature and calcite saturation states (Table 1). The average calcite saturation of 4.0 Ω for New Zealand is about double the average of 2.1 for the Antarctic localities (Takahashi et al., 2014). The two species of interest have different shell successions, with *L. uva* comprising primary and secondary layers, whereas *L. neozelanica* also has an additional tertiary layer (e.g., Peck et al., 1997; Williams, 1997; Goetz et al., 2009; Gaspard and Nouet, 2016; Table 1). The smaller, narrower, and rounder fibres with lower convexity of Antarctic *L. uva* should contain more organic matter than its counterpart *L. neozelanica* from New Zealand. This conclusion, boosted by the occurrence of a tertiary layer in *L. neozelanica*, agrees well with the observations of Peck and Edwards (1996), who reported that the shell of *L. uva* has a higher overall organic matter content than *L. neozelanica*.

The differences in the shell fabric and fibre size of the two species may be best explained by the environmental context where the two species evolved, with the Antarctic *L. uva* in seawater with lower carbonate saturation state than the temperate *L. neozelanica* (Watson et al., 2012). *L. uva* has a more organic rich secondary layer to cope with carbonate deposition in less favourable carbonate saturation conditions. It may also be adaptive in retarding shell dissolution under these conditions. Therefore, we conclude that there is a correlation between the size and shape of fibres of brachiopods and their ambient environment, especially with respect to seawater carbonate saturation, and temperature (Fig. 17).

6. Conclusions

Based on the analysis of the morphology and size of each fibre in the shells of six extant brachiopod species, we conclude that:

1) Morphometric parameters of ventral fibres are similar to those of dorsal valves when all species are considered. However, at the individual level, there are differences in morphometrics between dorsal and ventral valves that are related to a species-specific effect. In *G. vitreus* and *N. nigricans*, the fibres of the posterior external region of the ventral valve are significantly larger than those of the dorsal valve, possibly related to response to predation pressure.
2) There is an ontogenetic trend in the shape and size of the fibres: they become wider, larger, flatter, and less round with age.
3) This change in size and shape indicates that the fibrous layer produced in the late stage of growth may have a lower organic content compared to that produced first. The ontogenetic change in fibre morphometrics may be correlated to the observations that the anterior and inner parts of a shell are closer to isotopic equilibrium with seawater and are the best biogenic material for isotopic analysis.
4) An important consequence of the change in size and shape of the fibres with growth is that, in comparative studies of both recent and fossil shells, only shell portions produced at a similar ontogenetic stage should be sampled and compared.
5) The relationship between size and shape of fibres and environmental conditions is clear when comparing two species of the same genus living in seawater with different carbonate saturation state and temperature, but similar salinity. Notwithstanding their similarity at the TEM nanoscale, the fibres of *L. uva* are smaller, narrower, rounder and less convex than those of *L. neozelanica* at the microscale, contributing to the production of a more organic-rich shell, that may represent an adaptation for controlling carbonate deposition and countering shell dissolution in cold and less favourable carbonate saturation seawater conditions.

Acknowledgements

This project has received funding from the European Union's Horizon 2020 research and innovation programme under grant agreement No. 643084. We thank Curzio Malinverno and Agostino Rizzi for technical support. We thank two anonymous reviewers for their constructive comments.

References

Adams, D.C., Otarola-Castillo, E., 2013. Geomorph: an R package for the collection and analysis of geometric morphometric shape data. Methods Ecol. Evol. 4, 393–399.
Alvarez, M., Sanleón-Bartolomé, H., Tanhua, T., Mintrop, L., Luchetta, A., Cantoni, C., Schroeder, K., Civitarese, G., 2014. The CO_2 system in the Mediterranean Sea: a basin wide perspective. Ocean Sci. 10, 69–92.
Angiolini, L., Darbyshire, D.P.F., Stephenson, M.H., Leng, M.J., Brewer, T.S., Berra, F., Jadoul, F., 2007. Lower Permian brachiopods from Oman: their potential as climatic proxies. Earth. Env. Sci. Trans. R. Soc. 98, 327–344.
Angiolini, L., Jadoul, F., Leng, M.J., Stephenson, M.H., Rushton, J., Chenery, S., Crippa, G., 2009. How cold were the Early Permian glacial tropics? Testing sea-surface temperature using the oxygen isotope composition of rigorously screened brachiopod shells. J. Geol. Soc. 166, 933–945.
Auclair, A.C., Joachimski, M.M., Lécuyer, C., 2003. Deciphering kinetic, metabolic and environmental controls on stable isotope fractionations between seawater and the shell of *Terebratalia transversa* (Brachiopoda). Chem. Geol. 202, 59–78.
Brand, U., Logan, A., Bitner, M.A., Griesshaber, E., Azmy, K., Buhl, D., 2011. What is the ideal proxy of Palaeozoic seawater chemistry? Mem. Assoc. Australas. 41, 9–24.
Brand, U., Azmy, K., Griesshaber, E., Bitner, M.A., Logan, A., Zuschin, M., Ruggiero, E., Colin, P.L., 2015. Carbon isotope composition in modern brachiopod calcite: A case of equilibrium with seawater? Chem. Geol. 411, 81–96.
Brand, U., Azmy, K., Bitner, M.A., Logan, A., Zuschin, M., Came, R., Ruggiero, E., 2013. Oxygen isotopes and $MgCO_3$ in brachiopod calcite and a new paleotemperature equation. Chem. Geol. 359, 23–31.
Brand, U., Veizer, J., 1980. Chemical diagenesis of a multicomponent carbonate system-1: trace elements. J. Sed. Petrol 50, 1219–1236.
Brocas, W.M., Reynolds, D.J., Butler, P.G., Richardson, C.A., Scourse, J.D., Ridgway, I.D., Ramsay, K., 2013. The dog cockle, *Glycymeris glycymeris* (L.), a new annually-resolved sclerochronological archive for the Irish Sea. Palaeogeogr. Palaeoclimatol. Palaeoecol. 373, 133–140.
Core Team, R., 2016. R: A language and environment for statistical computing. R Foundation for Statistical Computing, Vienna, Austria URL https://www.R-project.org/.
Crippa, G., Angiolini, L., Bottini, C., Erba, E., Felletti, F., Frigerio, C., Hennissen, J.A.I., Leng, M.J., Petrizzo, M.R., Raffi, I., Raineri, G., Stephenson, M.H., 2016a. Seasonality fluctuations recorded in fossil bivalves during the early Pleistocene: Implications for climate change. Palaeogeogr. Palaeoclimatol. Palaeoecol. 446, 234–251.
Crippa, G., Ye, F., Malinverno, C., Rizzi, A., 2016b. Which is the best method to prepare invertebrate shells for SEM analysis? Testing different techniques on recent and fossil brachiopods. Boll. Soc. Paleontol. Ital. 55, 111–125.
Cross, E.L., Peck, L.S., Lamare, M.D., Harper, E.M., 2016. No ocean acidification effects on shell growth and repair in the New Zealand brachiopod *Calloria inconspicua* (Sowerby, 1846). ICES J. Mar. Sci. 73, 920–926.
Curry, G.B., Brunton, C.H., 2007. Stratigraphic distribution of brachiopods. In: Selden, P.A. (Ed.), Treatise on Invertebrate Paleontology. Part H, Revised, Brachiopoda. Geological Society of America and Paleontological Institute, Boulder, Colorado, and Lawrence, Kansa, USA, pp. 2901–3081.
Curry, G.B., Fallick, A.E., 2002. Use of stable oxygen isotope determinations from brachiopod shells in palaeoenvironmental reconstruction. Palaeogeogr. Palaeoclimatol. Palaeoecol. 182, 133–143.
Cusack, M., Huerta, A.P., 2012. Brachiopods recording seawater temperature-a matter of class or maturation? Chem. Geol. 334, 139–143.
Cusack, M., Parkinson, D., Pérez-Huerta, A., England, J., Curry, G.B., Fallick, A.E., 2007. Relationship between $\delta^{18}O$ and minor element composition of *Terebratalia transversa*. Earth. Env. Sci. Trans. R. Soc. 98, 443–449.
Delance, J.H., Emig, C.C., 2004. Drilling predation on *Gryphus vitreus* (Brachiopoda) off the French Mediterranean coasts. Palaeogeogr. Palaeoclimatol. Palaeoecol. 208, 23–30.
Duller, C., 2008. Teaching statistics with excel A big challenge for students and lecturers. Austrian J. Stat. 37, 195–206.
Garbelli, C., 2017. Shell microstructures in Upper Permian brachiopods: implication for fabric evolution and calcification. Riv. It. Paleont. Strat. 123, 541–560.
Garbelli, C., Angiolini, L., Jadoul, F., Brand, U., 2012. Micromorphology and differential preservation of Upper Permian brachiopod low-Mg calcite. Chem. Geol. 298, 1–10.
Garbelli, C., Angiolini, L., Brand, U., Jadoul, F., 2014. Brachiopod fabric, classes and biogeochemistry: implications for the reconstruction and interpretation of seawater carbon-isotope curves and records. Chem. Geol. 371, 60–67.
Garbelli, C., Angiolini, L., Shen, S.Z., 2017. Biomineralization and global change: a new perspective for understanding the end-Permian extinction. Geology 45 19–12.
Gaspard, D., Nouet, J., 2016. Hierarchical architecture of the inner layers of selected extant rhynchonelliform. J. Struct. Biol. 196, 197–205.
Głąb, T., Sadowska, U., Żabiński, A., 2015. Application of image analysis for grass tillering determination. Environ. Monit. Assess. 187, 674.
Goetz, A.J., Griesshaber, E., Neuser, R.D., Lüter, C., Hühner, M., Harper, E., Schmahl,

W.W., 2009. Calcite morphology, texture and hardness in the distinct layers of rhynchonelliform brachiopod shells. Eur. J. Mineral. 21, 303–315.
Goetz, A.J., Steinmetz, D.R., Griesshaber, E., Zaefferer, S., Raabe, D., Kelm, K., Irsen, S., Sehrbrock, A., Schmahl, W.W., 2011. Interdigitating biocalcite dendrites form a 3-D jigsaw structure in brachiopod shells. Acta Biomater. 7, 2237–2243.
Griesshaber, E., Job, R., Pettke, T., Schmahl, W.W., 2005. Micro-scale physical and chemical heterogeneities in biogenic materials – a combined micro-Raman, chemical composition and microhardness investigation. In: Katti, K., Ulm, F.J., Hellmich, C., Viney, C. (Eds.), Mechanical properties of bio-inspired and biological materials, MRS Symp. Proc. Series, Mater. Res. Soc. vol. 844, pp. 93–98.
Griesshaber, E., Kelm, K., Knieps, M., Schmahl, W.W., Job, R., Mader, W., 2006. The ultrastructure of brachiopod shells – a mechanically optimized material with hierarchical architecture. In: Mater. Res. Soc. Symp. Proc., 989E, 0898-L12-01.
Griesshaber, E., Schmahl, W.W., Neuser, R., Pettke, T., Blum, M., Mutterlose, J., Brand, U., 2007. Crystallographic texture and microstructure of terebratulide brachiopod shell calcite: An optimized materials design with hierarchical architecture. Am. Mineral. 92, 722–734.
Griesshaber, E., Neuser, R.D., Brand, U., Schmahl, W.W., 2008. Texture and microstructure of modern rhynchonellide brachiopod shells – an ontogenetic study. Proc. ICOTOM 15 Conference. Am. Ceram. Soc. 201, 605–619.
Griesshaber, E., Neuser, R.D., Schmahl, W.W., 2010. The application of EBSD analysis to biomaterials: microstructural and crystallographic texture variations in marine carbonate shells. Semin. Soc. Esp. Mineral. 07, 22–34.
Grossman, E.L., Zhang, C., Yancey, T.E., 1991. Stable-isotope stratigraphy of brachiopods from Pennsylvanian shales in Texas. Geol. Soc. Am. Bull. 103, 953–965.
Grossman, E.L., Mii, H.S., Zhang, C., Yancey, T.E., 1996. Chemical variation in Pennsylvanian brachiopod shells; diagenetic, taxonomic, microstructural, and seasonal effects. J. Sediment. Res. 66, 1011–1022.
Harper, E.M., Peck, L.S., 2016. Latitudinal and depth gradients in marine predation pressure. Glob. Ecol. Biogeogr. 25, 670–678.
Harper, E.M., Robinson, J.H., Lee, D.E., 2011. Drill hole analysis reveals evidence of targeted predation on modern brachiopods. Palaeogeogr. Palaeoclimatol. Palaeoecol. 305, 162–171.
Immenhauser, A., Schöne, B.R., Hoffmann, R., Niedermayr, A., 2016. Mollusc and brachiopod skeletal hard parts: Intricate archives of their marine environment. Sedimentology 63, 1–59.
Klingenberg, C.P., Barluenga, M., Meyer, A., 2002. Shape analysis of symmetric structures: quantifying variation among individuals and asymmetry. Evolution 56, 1909–1920.
Lowenstam, H.A., 1961. Mineralogy, O^{18}/O^{16} ratios, and strontium and magnesium contents of recent and fossil brachiopods and their bearing on the history of the oceans. J. Geol. 69, 241–260.
Mardia, K.V., Bookstein, F.L., Moreton, I.J., 2000. Statistical assessment of bilateral symmetry of shapes. Biometrika. 87, 285–300.
Palmer, A.R., 1992. Calcification in marine molluscs: how costly is it? Proc. Natl. Acad. Sci. U.S.A. 89, 1379–1382.
Parkinson, D., Curry, G.B., Cusack, M., Fallick, A.E., 2005. Shell structure, patterns and trends of oxygen and carbon stable isotopes in modern brachiopod shells. Chem. Geol. 219, 193–235.
Peck, L.S., 2007. Brachiopods and climate change. Earth. Env. Sci. Trans. R. So. 98, 451–456.
Peck, L.S., Edwards, T.M., 1996. Organic contents and elemental composition of brachiopod shell and mantle tissues, in: Cooper, P., Jin, J. (Eds.), Brachiopods. Proceedings of the Third International Brachiopod Congress, Sudbury, Ontario, Canada, September 1995. Brookfield, VT: A.A. Balkema, Rotterdam, Netherlands, pp. 203–207.
Peck, L.S., Rhodes, M.C., Curry, G.B., Ansell, A.D., 1997. Physiology. In: Kaesler, R.L. (Ed.), Treatise on Invertebrate Paleontology. Part H, Revised, Brachiopoda. Geological Society of America Inc., and The University of Kansas, Boulder, Colorado, USA, pp. 213–242.
Peck, L.S., 2001. Ecology (Chapter 11), in: Carlson, S., Sandy, M. (Eds.), Brachiopods ancient and modern: a tribute to G. Arthur Cooper. The Paleontology Society Papers, and the Yale University, New Haven, Connecticut, USA, pp. 171–183.
Penman, D.E., Hönisch, B., Rasbury, E.T., Hemming, N.G., Spero, H.J., 2013. Boron, carbon and oxygen isotope composition of brachiopod shells: intra-shell variability, controls, and potential as a paleo-pH recorder. Chem. Geol. 340, 32–39.
Pérez-Huerta, A., Cusack, M., Zhu, W., England, J., Hughes, J., 2007. Material properties of brachiopod shell ultrastructure by nanoindentation. J. R. Soc. Interface 4, 33–39.
Pérez-Huerta, A., Cusack, M., McDonald, S., Marone, F., Stampanoni, M., MacKay, S., 2009. Brachiopod punctae: a complexity in shell biomineralisation. J. Struct. Biol. 167, 62–67.
Popp, B.N., Anderson, T.F., Sandberg, P.A., 1986. Brachiopods as indicators of original isotopic compositions in some Paleozoic limestones. Geol. Soc. Am. Bull. 97, 1262–1269.
Randle, V., Engler, O., 2000. Introduction to Texture Analysis: Macrotexture, Microtexture and Orientation Mapping. CRC Press, Amsterdam.
Rollion-Bard, C., Saulnier, S., Vigier, N., Schumacher, A., Chaussidon, M., Lécuyer, C., 2016. Variability in magnesium, carbon and oxygen isotope compositions of brachiopod shells: implications for paleoceanographic studies. Chem. Geol. 423, 49–60.
Rosenberg, G.D., Hughes, W.W., Tkachuck, R.D., 1988. Intermediary metabolism and shell growth in the brachiopod *Terebratalia transversa*. Lethaia 21, 219–230.
Russ, J.C., Neal, F.B., 2015. The Image Processing Handbook (7th ed.). Boca Raton.
Schmahl, W.W., Griesshaber, E., Neuser, R., Lenze, A., Job, R., Brand, U., 2004. The microstructure of the fibrous layer of terebratulide brachiopod shell calcite. Eur. J. Mineral. 16, 693–697.
Schmahl, W.W., Griesshaber, E., Merkel, C., Kelm, K., Deuschle, J., Neuser, R.D., Göetz, A.J., Sehrbrock, A., Mader, W., 2008. Hierarchical fibre composite structure and micromechanical properties of phosphatic and calcitic brachiopod shell biomaterials – an overview. Mineral. Mag. 72, 541–562.
Schmahl, W.W., Griesshaber, E., Kelm, K., Goetz, A., Jordan, G., Ball, A., Xu, D., Merkel, C., Brand, U., 2012. Hierarchical structure of marine shell biomaterials: biomechanical functionalization of calcite by brachiopods. Z. Kristallog. Cryst. Mater. 227, 793–804.
Schmidt, N.H., Olesen, N.O., 1989. Computer-aided determination of crystal-lattice orientation from electron channeling patterns in the SEM. Can. Mineral. 27, 15–22.
Schöne, B.R., Surge, D.M., 2012. Part N, Revised, Volume 1, Chapter 14: Bivalve sclerochronology and geochemistry. Treat. Online 46, pp. 1–24.
Takahashi, T., Sutherland, S.C., Chipman, D.W., Goddard, J.G., Ho, C., Newberger, T., Sweeney, C., Munro, D.R., 2014. Climatological distributions of pH, pCO_2, total CO_2, alkalinity, and $CaCO_3$ saturation in the global surface ocean, and temporal changes at selected locations. Mar. Chem. 164, 95–125.
Watson, S.A., Peck, L.S., Tyler, P.A., Southgate, P.C., Tan, K.S., Day, R.W., Morley, S.S., 2012. Marine invertebrate skeleton size varies with latitude, temperature and carbonate saturation: implications for global change and ocean acidification. Glob. Chang. Biol. 18, 3026–3038.
Williams, A., 1966. Growth and structure of the shell of living articulate brachiopods. Nature 211, 1146–1148.
Williams, A., 1968. Evolution of the shell structure of articulate brachiopods. Spec. Pap. Palaeontol. 2, 1–55.
Williams, A., 1997. Shell structure. In: Kaesler, R.L. (Ed.), Treatise on Invertebrate Paleontology. Part H, Revised, Brachiopoda. Geological Society of America Inc., and The University of Kansas, Boulder, Colorado, USA, pp. 267–320.
Yamamoto, K., Asami, R., Iryu, Y., 2011. Brachiopod taxa and shell portions reliably recording past ocean environments: toward establishing a robust paleoceanographic proxy. Geophys. Res. Lett. 38, L13601. http://dx.doi.org/10.1029/2011GL047134.
Yamamoto, K., Asami, R., Iryu, Y., 2013. Correlative relationships between carbon-and oxygen-isotope records in two cool-temperate brachiopod species off Otsuchi Bay, northeastern Japan. Paleontol. Res. 17, 12–26.
Ye, F., Crippa, G., Garbelli, C., Griesshaber, E., 2017. Microstructural data of six recent brachiopod species: SEM, EBSD, morphometric and statistical analyses. Data in Brief submitted.
Zuschin, M., Stachowitsch, M., Stanton Jr, R.J., 2003. Patterns and processes of shell fragmentation in modern and ancient marine environments. Earth. Sci. Rev. 63, 33–82.